Copyright © 2009 by ABCM

A FINITE ELEMENT NUMERICAL SIMULATION OF THE LAMINAR FLOW OVER AN OSCILLATING AIRFOIL

Luciano Gonçalves Noleto, lucianonoleto@unb.br
Antonio C. P. Brasil Junior, brasiljr@unb.br
Universidade de Brasília, Faculdade de Tecnologia, Departamento de Engenharia Mecânica, Laboratório de Energia e Ambiente, 70910-900 - Asa Norte - Brasília, DF - Brasil

Manuel Nascimento Dias Barcelos Júnior
Universidade de Brasília, Faculdade UnB Gama, Área Especial 2 Lote 14 Setor Central Gama-DF

Abstract. *: This paper presents results of a numerical simulation of the laminar flow over a NACA 0012 airfoil. Its goal is to observe the dynamic stall phenomena. Recurring phenomena linked to the flow over moving boundaries are transition to turbulence, boundary layer separation and dynamic stall. Among these informations, numerical simulation of the flow profile is a suitable tool to acquire knowledge over the mentioned phenomena. A finite element code will be employed to conduct the numerical simulation. An explicit projection method will be employed at the simulation, with P1 triangular grid elements. Also, this work will employ the CBS stabilization scheme. In a first approach, the airfoil will be simulated in a static condition to assess the lift acting on the airfoil, and compare it with experimentation. Thus, the airfoil will be submitted into an oscillating pattern in order to observe the dynamic stall. For the moving boundary, an Arbitrary Eulerian Lagrangean (ALE) scheme will be employed to contemplate mesh deformation. The ALE method has the ability to control mesh geometry independently from material geometry. The results obtained will be showed with velocity vectors*

Keywords: *Oscillating Airfoil, finite element method, projection method, ALE scheme.*

1. INTRODUCTION

Flows over moving boundaries are common in engineering. Flame propagation, oil recovery, runners and vanes of turbomachines, keels of boats, dam ruptures and explosions are examples (Shyy et al. (2008)). On bioengineering one can count the blood flow at veins and arteries and airflow inside the lungs as example of this kind of flow. Here, the moving boundary and the flow can influence each other's mechanics, causing vibration or strains in solids, or generating instabilities that can lead to turbulence in fluids. Besides, chemical processes, phase changing can be fitted inside this kind of flow. Usually, the moving boundary is considered, under the continuum mechanics point of view, as a discontinuity, which can generates to grid generation problems. The Dynamic stall can be characterized by an airfoil oscillating in pitching or plunging motion. If the angle of attack of the airfoil surpasses the stall angle, a large gain in lift is observed, with increases in drag and negative moments are applied by the flow into the airfoil. The flow separation is delayed, due to the time scale differences between inviscid and viscous phenomena. Its effects can be seen in aerodynamics, hydro and wind turbines, helicopter rotors and aircraft engines. Recurring phenomena in dynamic stall are: unsteady separation, shear layer instabilities and shock-boundary layer interaction (Digavallis (1993)). There are several numerical methods to study this kind flow, such as SPH (Smooth Particle Hydrodynamics), VOF (Volume of Fluid), Immersed Boundary method and the Arbitrary Lagrangean-Eulerian method (Duan and Li, 2007), which will be used in this paper.

On a very simple definition, the finite element method is a method that works with local base functions, which are multiplied by weight functions and integrated over a domain ((Zienkiewicz, 2005a, Franca et al.,2006, Donea and Huerta, 2003). Its main advantages are the applications to complex geometries, easy implementation of interpolation schemes and its solid mathematical foundations. On the other hand, its main challenge is the determination of a weak form of the problem that accurately represents the strong form of the same problem, as well as the insurance of stabilization of the advective term in fluid mechanics applications. One example of stabilization scheme is the CBS (Characteristic Based Split) method (Pereira, 2004, Zienkiewicz, 2005b). One can state that the CBS method uses features of projection methods and characteristic methods. The stabilization is achieved by splitting the pressure terms of the Navier-Stokes equation, considering it as a source term. Therefore, it is calculated apart from the remaining terms of the equation.

This paper will perform a numerical simulation of the laminar flow over the oscillating NACA 0012 airfoil with the ALE method to contemplate the moving airfoil. An in-house finite element code will be employed for the calculations. Results of the simulation for several angles of attack in a static fashion will be showed. The lift coefficient will be calculated and compared with experimentation for the attack angles. For the dynamic airfoil movement, qualitative results of the flow with the oscillating airfoil will be presented in order to characterize the dynamic stall pattern.

2. MATHEMATICAL FORMULATION

Let us consider a time dependent laminar and incompressible fluid flow problem described as follows: Find the velocity and pressure fields $\mathbf{u}(\mathbf{x},t)$ and $p(\mathbf{x},t)$ defined in $\Omega_t \times [0,T]$, where Ω_t is a bounded open subset of $\mathbb{R}^d$ (d=2 or 3) with boundary $\Gamma_t = \partial\Omega_t$, varying both on time, such that:

$$\nabla.\mathbf{u} = \mathbf{0} \tag{1}$$

$$\frac{\partial \mathbf{u}}{\partial t} + (\nabla \mathbf{u})\mathbf{u} = -\frac{\mathbf{1}}{\rho}\nabla \mathbf{p} + \nu \nabla^{\mathbf{2}}\mathbf{u} + \mathbf{f} \tag{2}$$

In these equations ρ and ν denote the density and viscosity of the fluid and $\mathbf{f}$ is a given forcing function.

Taken into account the time-dependency of Ω_t, the Arbitrary Lagrangian-Eulerian (ALE) approach is used in order to describe flow variables in a context of moving domains. Let χ_t a invertible mapping function which for all t mapps a point $\mathbf{X} \in \Omega_0$ to a point $\mathbf{x} = \chi_t(\mathbf{X}) \in \Omega_t$, with:

$$\begin{array}{rccl} \chi_t: & \Omega_0 & \mapsto & \Omega_t; \\ & \mathbf{X} & \mapsto & \mathbf{x} = \chi_t(\mathbf{X}) \end{array} \tag{3}$$

The domain velocity is computed using χ_t as follows:

$$\mathbf{w}(\mathbf{x},t) = \left.\frac{\partial \chi_t}{\partial t}\right|_{\mathbf{x}} (\mathbf{x},t) \tag{4}$$

Considering now the ALE mapping, for any function $f : \Omega_t \mapsto \mathbb{R}$ the material derivative can be written as:

$$\left.\frac{df}{dt}\right|_{\mathbf{x}} = \frac{\partial f}{\partial t}(\mathbf{x},t) + \mathbf{w}(\mathbf{x},t).\nabla f(\mathbf{x},t) \tag{5}$$

Finally, the continuity and momentum laws are reformulated in a referencial description, transformed the original problem (1)-(2) to: Find the velocity and pressure fields $\mathbf{u}(\mathbf{x},t)$ and $p(\mathbf{x},t)$ defined in $\Omega_t \times [0,T]$, such that:

$$\nabla.\mathbf{u} = \mathbf{0} \tag{6}$$

$$\frac{\partial \mathbf{u}}{\partial t} + (\nabla \mathbf{u})\hat{\mathbf{u}} = -\frac{\mathbf{1}}{\rho}\nabla \mathbf{p} + \nu \nabla^{\mathbf{2}}\mathbf{u} + \mathbf{f} \tag{7}$$

to those equations $\hat{\mathbf{u}} = \mathbf{u} - \mathbf{w}$ denote the relative fluid velocity and initial conditions are added:

$$\mathbf{u}(\mathbf{x},0) = \mathbf{u}_0 \;\; ; \;\; p(\mathbf{x},0) = p_0 \quad \text{in} \quad \Omega_0 \tag{8}$$

and the boundary conditions are defined on $\Gamma_t = \Gamma_d \cup \Gamma_{w,t} \cup \Gamma_o$ as:

$$\mathbf{u}(\mathbf{x},t) = \mathbf{u}_d; \quad \text{on} \quad \Gamma_d \tag{9}$$

$$\mathbf{u}(\mathbf{x},t) = \mathbf{w}; \quad \text{on} \quad \Gamma_{w,t} \tag{10}$$

$$p(\mathbf{x},t) = p_{\text{ref}}; \quad \text{on} \quad \Gamma_o \tag{11}$$

For those conditions Γ_d represents the part of the boundary which is maintained fixed on time and where Dirichlet boundary conditions for the velocity field are prescribed. $\Gamma_{w,t}$ is the moving boundary, where the fluid velocity is equivalent to the domain velocity. Γ_o is the outlet boundary where a reference pressure is prescribed (see Fig. 1).

Remark: In the present work the domain kinematic is defined only from the motion of one part of the boudary $\Gamma_{w,t}$ (related to the tilting of airfoil). The prescribed motion of the moving boundary defines the geometrical motion of the domain (mapping function χ_t) as well as its local velocity ($\mathbf{w}(\mathbf{x},t)$). It can be expressed by a mathematical problem: Find $\mathbf{x}(\mathbf{X},t)$ such that:

$$\mathcal{L}(\mathbf{x}) = 0 \tag{12}$$

with boundary conditions prescribed on $\Gamma_{w,t}$ as $\mathbf{x} = \mathbf{x}_w$. $\mathcal{L}(.)$ denotes a mathematical operator related to the mapping χ_t due the domain deformation.

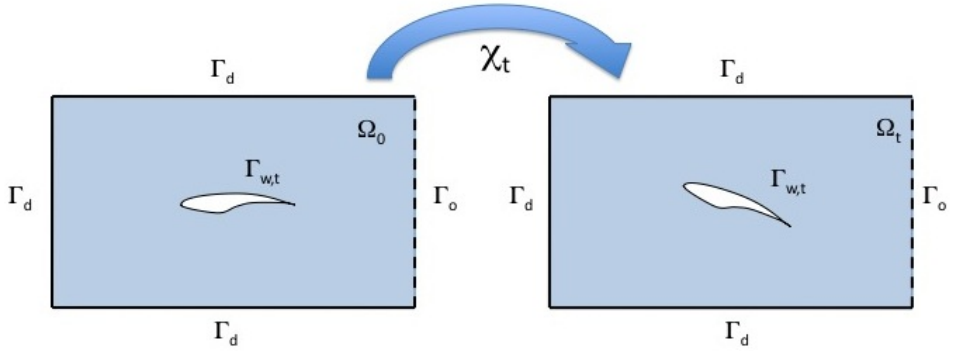

Figure 1. Moving domain with an oscilating airfoil

3. Numerical Methods

3.1 Time Discretization - Projection Algorithm

The present methodology is designed for the semi-explicit iterative solution of system (6)-(7) after time and spatial discretization, considering a framework of projection methods (e.g. Chorin (1968), Guermond et al. (2006), Goldberg and Ruas (1999), Lohner et al. (2006)).

Let $\Delta t > 0$ be a given time step. Considering the set of variables known in a previous time step t, denoted by $(\mathbf{u}^n, p^n, \mathbf{x}^n, \mathbf{w}^n)$, the solution at time $t + \Delta t$, $(\mathbf{u}^{n+1}, p^{n+1}, \mathbf{x}^{n+1}, \mathbf{w}^{n+1})$ can be obtained from the following splitting approach:

$$\frac{1}{\Delta t}\left(\mathbf{u}^* - \mathbf{u}^n\right) + (\nabla \mathbf{u}^n)\hat{\mathbf{u}}^n = -\frac{1}{\rho}\nabla p^n + \nu \nabla^2 \mathbf{u}^n + \mathbf{f} \tag{13}$$

$$\frac{1}{\Delta t}\left(\mathbf{u}^{n+1} - \mathbf{u}^*\right) = -\frac{1}{\rho}\nabla(p^{n+1} - p^n) \tag{14}$$

$$\nabla.\mathbf{u}^{n+1} = 0 \tag{15}$$

$$\mathcal{L}(\mathbf{x}^{n+1}) = 0 \;\; ; \;\; \mathbf{w}^{n+1} = \frac{1}{\Delta t}\left(\mathbf{x}^{n+1} - \mathbf{x}^n\right) \tag{16}$$

The fractional-step algorithm introduces a predicted velocity $\mathbf{u}^*$, which is corrected on the end of steps.
Taking the divergence of the equation (14) and using (15) the pressure-Poisson equation can be obtained:

$$\nabla^2\left(p^{n+1} - p^n\right) = \frac{\rho}{\Delta t}\nabla.\mathbf{u}^* \tag{17}$$

The boundary conditions for this equation has to be considered as follows:

$$\nabla\left(p^{n+1} - p^n\right).\mathbf{n} = \frac{\rho}{\Delta t}\mathbf{u}^*.\mathbf{n} \;\text{ on } \Gamma \tag{18}$$

Remark: The projection algorithm used here is called Incremental Projection Scheme. It is a modification of the classical version proposed by Chorin (1968). This implementation improve the convergence properties as reported in literature (Guermond et al. (2006) , Codina (2000)).

3.2 Standard Weak Form

As usual, we denote $L^2(\Omega_t)$ the space of functions that are squared integrable over the domain Ω_t and $H^1(\Omega_t)$ the Sobolev space whose the derivatives are also squared integrables. A bold character is used for vector-valued functions of those spaces. The $L^2(\Omega_t)$ internal product is denoted by $(.,.) = \int_{\Omega_t} .. \, d\Omega_t$ and $H^1_0(\Omega_t)$ is the sub-space of function with zero value on boundaries.

Given weight functions $\mathbf{v} \in V = H^1_0(\Omega_t)$ and $q \in Q = L^2(\Omega_t)/\mathbb{R}$. Considering also $\mathbf{u} \in U = H^1(\Omega_t)$. The weak form of the equations (13), (17) and (14) can be written as follows:

$$m(\boldsymbol{\Delta}\mathbf{u}^*, \mathbf{v}) + c(\mathbf{u}^n, \hat{\mathbf{u}}^n, \mathbf{v}) + \nu\, a(\mathbf{u}^n, \mathbf{v}) + \frac{1}{\rho} b(p, \mathbf{v}) = (\mathbf{f}, \mathbf{v}) \tag{19}$$

$$a(\Delta p, q) = -\frac{\rho}{\Delta t}\, b(\mathbf{u}^*, q) \tag{20}$$

$$m(\boldsymbol{\Delta}\mathbf{u}^{n+1}, \mathbf{v}) = -\frac{1}{\rho}\, b(\Delta p, \mathbf{v}) \tag{21}$$

where the following forms are introduced

$$m(\mathbf{u}, \mathbf{v}) := \frac{1}{\Delta t}(\mathbf{u}, \mathbf{v})\ ;\ c(\mathbf{u}, \mathbf{w}, \mathbf{v}) := ((\nabla.\mathbf{u})\mathbf{w}, \mathbf{v}) \tag{22}$$

$$a(\mathbf{u}, \mathbf{v}) := (\nabla\mathbf{u}, \nabla\mathbf{v})\ ;\ b(q, \mathbf{v}) := (q, \nabla.\mathbf{v}) \tag{23}$$

The increments of velocity and pressure fields at each spliting step are denoted by $\boldsymbol{\Delta}\mathbf{u}^* = \mathbf{u}^* - \mathbf{u}^n$, $\boldsymbol{\Delta}\mathbf{u}^{n+1} = \mathbf{u}^{n+1} - \mathbf{u}^*$ and $\Delta p = p^{n+1} - p^n$.

Remark: The proposed methodology is based in a fractional-step scheme with a simple first order discretization on time. The incremental solution at each time step of the equations (19)-(21) leads to the consistent formulation for the fields at $t + \Delta t$. In a framework of ALE method, the problem has to be complemented by the kinetic formulation of the moving domain. It will be dicussed later.

3.3 Finite Element Discretization

Let $T^h(\Omega_t)$ a regular partition of the domain Ω_t from which the finite element spaces $Q_h \subset Q$, $V_h \subset V$ and $U_h \subset U$ are constructed. The discrete problem equivalent to the weak form can be written as: Given $\{\mathbf{u}_h^n, p_h^n, \mathbf{w}_h^n\}$, find $\{\mathbf{u}_h^{n+1}, p_h^{n+1}\} \in U_h \times Q_h$ such that $\forall\ \{\mathbf{v_h}, q_h\} \in V_h \times Q_h$:

$$\begin{aligned} m(\boldsymbol{\Delta}\mathbf{u}_h^*, \mathbf{v}_h) \quad &= \quad -c(\mathbf{u}_h^n, \hat{\mathbf{u}}_h^n, \mathbf{v}_h) - \nu\, a(\mathbf{u}_h^n, \mathbf{v}_h) - && (24)\\ &\quad -\frac{1}{\rho}\, b(p_h, \mathbf{v}_h) - s(\mathbf{u}_h^n, \hat{\mathbf{u}}_h^n, \mathbf{v}_h) + (\mathbf{f}, \mathbf{v}_h) && (25)\end{aligned}$$

$$a(\Delta p_h, q_h) = -\frac{\rho}{\Delta t} b(\mathbf{u}_h^*, q_h) \tag{26}$$

$$m(\boldsymbol{\Delta}\mathbf{u}_h^{n+1}, \mathbf{v}_h) = -\frac{1}{\rho}\, b(\Delta p_h, \mathbf{v}_h) \tag{27}$$

An extra term is added to the discrete form (25), to assure the stability for convection dominated regimes. This term is given by:

$$s(\mathbf{u}_h^n, \hat{\mathbf{u}}_h^n, \mathbf{v}_h) = ((\nabla\mathbf{u}_h^n)\hat{\mathbf{u}}_h^n, \Delta t(\nabla\mathbf{v})\hat{\mathbf{u}}_h^n) \tag{28}$$

Considering the dimension of the spaces given by $dim(V_h) = dim(U_h) = dim(Q_h) = N$ and base function respectivelly denoted by $\{\mathbf{N}_i; i = 1, N\}$ and $\{N_i; i = 1, N\}$, the matrix form of the discrete problem are written as:

Step 1: Predict velocity by Momentum equation

$$\mathbf{M}.\boldsymbol{\Delta}\mathbf{u}_h^* = \mathbf{F}_u^*(\mathbf{u}_h^n, \mathbf{w}_h^n, p_h^n) \tag{29}$$

Step 2: Pressure-Poisson problem

$$\mathbf{A}.\Delta p_h = \mathbf{F}_p(\mathbf{u}_h^*) \tag{30}$$

Step 3: Velocity correction - Projection in divergence free space

$$\mathbf{M}.\boldsymbol{\Delta}\mathbf{u}_h^{n+1} = \mathbf{F}_u(\Delta p_h) \tag{31}$$

In those equations $\mathbf{M}$ and $\mathbf{A}$ are the mass and discrete Laplacian matrices given by:

$$\mathbf{M}_{ij} = \frac{1}{\Delta t}(\mathbf{N}_i, \mathbf{N}_j)\ \ ;\ \ \mathbf{A}_{i,j} = (\nabla N_i, \nabla N_j) \tag{32}$$

The vectors $\mathbf{F}_u^*$, $\mathbf{F}_p$ and $\mathbf{F}_u$ are related to the discretization of the right hand side of the matrix equations on the steps 1-3. The boundary integral terms (related to the boundary conditions) are added into these vectors.

Remarks:

- The solution of the linear systems at steps 1 and 3 involve the mass matrix. In order to enhance the convergence rate of the computations, this matrix is lumped in a diagonal form. It is performed once in the beginning of the iterative computation.
- The linear system for the pressure correction problem, step2, is solved by the Conjugated Gradient Method, preconditioning by partial Cholesky factorization. This matrix is stored by a space Morse strategy, and the preconditioning is also performed once when this matrix is firstly computed.
- In the present paper the time step is controlled by the following expression:

$$\Delta t \leqslant \frac{\Delta t_{adv} \Delta t_{diff}}{\Delta t_{adv} + \Delta t_{diff}} \tag{33}$$

3.4 Moving Mesh Methodology

The governing equation of the motion of the fluid mesh is built considering the fluid mesh as a pseudo-elastic structure (Batina(1991), Koobus et al.(1998), Degand and Farhat(2002), Farhat et al.(1998))

$$\mathcal{L}(\mathbf{x}) = \mathbf{M}\ddot{x} + \mathbf{C}\dot{x} + \mathbf{K}x - \mathbf{R} \tag{34}$$

where **M**, **C** and **K** are respectively the fictitious mass, damping and stiffness matrices associated to the fluid grid and **R** is the reaction force. For a quasi-static model the fictitious mass **M** and damping **C** matrices are neglected, resulting in:

$$\mathcal{L}(\mathbf{x}) = \mathbf{K}x - \mathbf{R} \tag{35}$$

The quasi-static approach, due to its simplified structure and solution strategy, is usually preferred for the modeling of fluid-structure interaction problems. The quasi-static fluid mesh motion equations obey the kinematic compatibility between fluid and structure. The kinematic compatibility dictates how the position x_Γ of fluid mesh on the boundary Γ is related to the fluid mesh boundary velocity v_Γ by:

$$x_\Gamma = \Delta t v_\Gamma \tag{36}$$

where Δt is fluid problem time step. For this problem the fluid mesh boundary points have a uniform rotation movement of radius **r** with respect to a specified center point. Therefore, the fluid boundary moves as if there was a rigid structure rotating with a constant angular velocity ω.

$$v_\Gamma = \omega \mathbf{r} \tag{37}$$

The fictitious stiffness matrix **K** and the reaction force vector **R** in equation can be divided in subsets related to the internal (Γ) and external (Ω) degrees of freedom of the fluid mesh:

$$\begin{bmatrix} \mathbf{K}_{\Omega\Omega} & \mathbf{K}_{\Omega\Gamma} \\ \mathbf{K}_{\Gamma\Omega} & \mathbf{K}_{\Gamma\Gamma} \end{bmatrix} \begin{bmatrix} x_\Omega \\ x_\Gamma \end{bmatrix} - \begin{bmatrix} \mathbf{R}_\Omega \\ \mathbf{R}_\Gamma \end{bmatrix} = \mathcal{L}(\mathbf{x}) \tag{38}$$

Equation 5 is solved with the condition of null force on the internal grid points ($\mathbf{R}_\Omega = 0$). Also, in this work for the fluid mesh motion problem, a quasi-static model is used as described in equation 2, and the fictitious stiffness matrix **K** is constructed by an improved spring analogy method (Koobus et al.(1998)). As the main goal is to deal with fluid-structure interaction problems of small to medium scale, the solution strategy employs a direct method to solve the mesh motion linear system of equations. The direct method is preferred because of its simplicity and robustness.

3.5 Boundary Conditions

At the inlet, the velocity was set to match a Reynolds number of 10^3. The outlet boundary condition has a zero reference pressure, and the airfoil wall was imposed the mesh velocity, in order to recover a fluid velocity equal to zero at the ALE equations. The used grid has 1761 nodes and 3198 P1 elements. In the static case, the NACA 0012 airfoil were simulated in several angles of attack to validate the flow pattern and the vertical force coefficient. In the dynamic case, the airfoil is pitched up to 20 degrees and then, pitched down to 7 degrees, in order to observe the flow pattern of the dynamic stall.

The lift coefficient is the non-dimensional lift force, given as follows (Naudascher and Rockwell (2005)):

$$C_l = \frac{F_l}{0.5\rho u^2 A} \tag{39}$$

Where A is the airfoil surface area, calculated with the element face that composes the airfoil surface. The used grid is displayed in figure 2

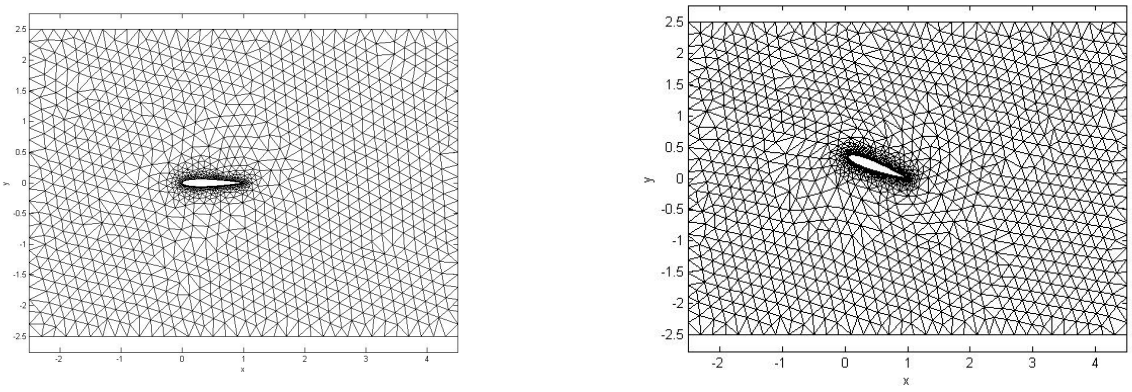

Figure 2. Discretization detail and Deformed mesh

4. RESULTS

4.1 Static Airfoil

The results obtained for the static simulation shows that the developed code was able to predict the lift coefficient with good precision below 8 degrees of attack angle (Figure 3). Above that angle, the results start to overestimate, when compared with the experimental results present in Naudascher and Rockwell (2005). One can state that this overestimate is due to stall effects, since the NACA 0012 has its normal stall around 10 degrees for the Reynolds Number used for this work. At this condition, boundary layer detachment occurs due to pressure gradients originated by the angulation of the airfoil. Also, in laminar flow, coherent structures can be emitted from the airfoil in a high attack angle. The velocity vectors at figures 4 and 5 shows that trend. At 8 degrees, recirculation zones appears close to the airfoil's trailing edge. Those zones begin to grow and generate a vortex wake downstream at the subsequent higher angles, where at 20 degrees the wake and the recirculation zone begin to shows signs of instability due to the gradient pressure generated by the airfoil angulation. These patterns are observed at the reference, where the 12 degrees display can be fitted into a light stall, where a separation bubble is noted at the leading edge and the flow is separated close to the trailing edge. The 20 degrees vector display shows similarity with a deep stall regime, where a big recirculation zone is noted, and vortex wake is generated downstream (Svacek et al. (2007)).

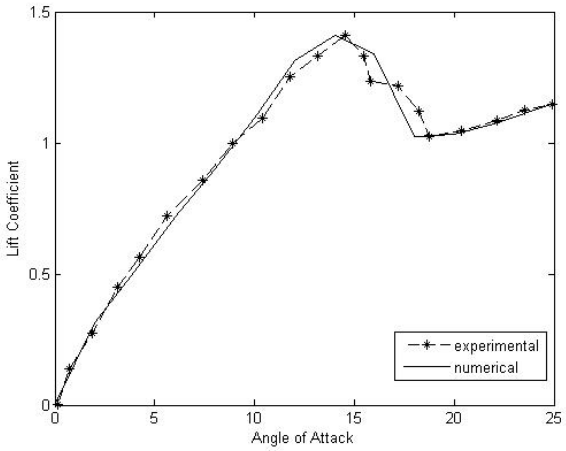

Figure 3. Static Lift Coefficient Curve

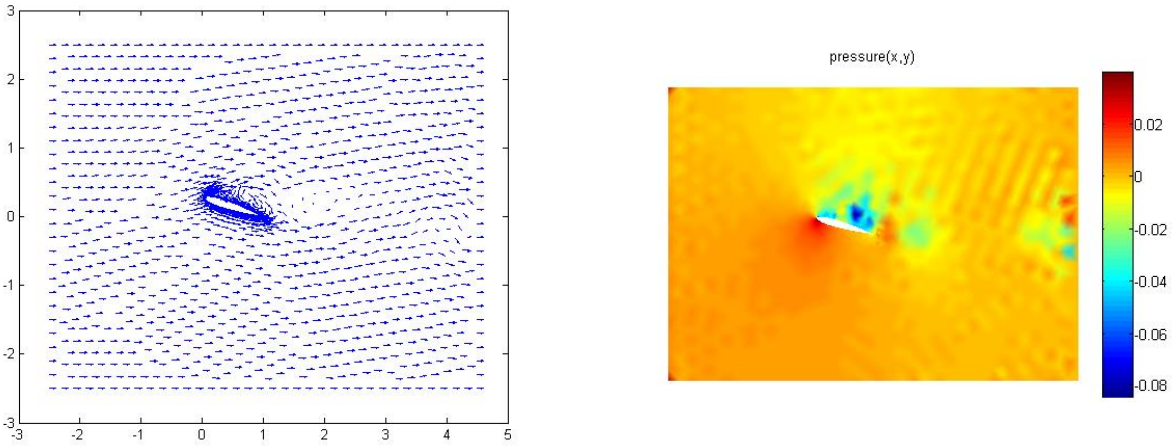

Figure 4. Velocity Vectors and Pressure Contours at 16 degrees

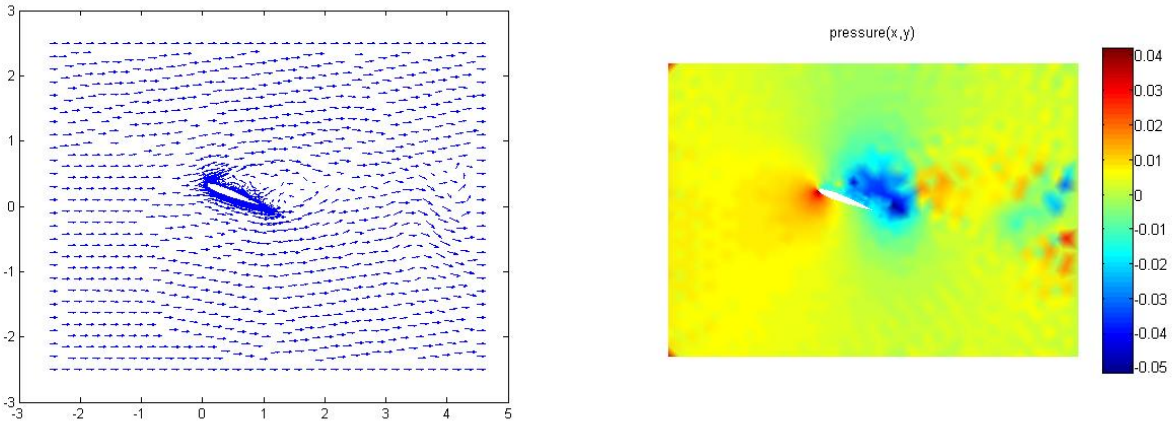

Figure 5. Velocity Vectors and Pressure Contours at 20 degrees

4.2 Moving Airfoil

The velocity vectors and pressure contours showed in figures 6, 7 and 8 shows the dynamic stall pattern. The flow topology bears close similarity with the visualization results displayed at Naudascher and Rockwell (2005) and Svacek et al. (2007). In a pitching airfoil condition where the angle of attack increases, the boundary layer is fully attached at the lower surface of the airfoil, while the upper surface shows that the separation point moves upstream (figure 6). The presented flow topology is a free shear layer wake at the trailing edge, while the vorticity assumes a counterclockwise shedding pattern, which is consistent with the increasing airfoil circulation. One can note that on this phase of increasing angle of attack, the separation point remains moving upstream, until it reaches the leading edge (Digavallis (1993), Fujisawa and Shibuya (2001)). The shear layer at the upper surface rolls up, configuring the dynamic stall pattern, identified by a primary vortex formed. This vortex became bigger as it departs from the airfoil to, finally, detaches itself. At that moment, the shear layer that is emitted from the trailing edge gains force, to generate the counterclockwise shedding mentioned before. At that moment, the normal force reaches its maximum value. When the angle of attack starts decreasing (figures 7, 8 and 9). The primary vortex moves downstream and the separation point moves toward the trailing edge, where the vortex is drifted downstream and a negative vorticity is generated by a shear layer modified by the down-pitching ((Digavallis (1993), Ekaterinas and Platzer (1997)). This vorticity is shed from the trailing edge . At the pitching down, the boundary layer reattaches to the airfoil's upper surface. Figure 10 shows the dynamic lift coefficient curve. The data displayed on this curve has resemblance from figure 2, which displays static data. One can notice the quasi-hysteretic behavior of the lift, where the pitching down curve shows more variation on the lift when compared with the pitching up curve. One can note that turbulence and compressibility effects affects the dynamic stall. In turbulence, the flow pattern resembles the laminar pattern, while in compressible flow, a supersonic region is developed over the airfoil, which is halted by a normal shockwave that interacts with the boundary layer.

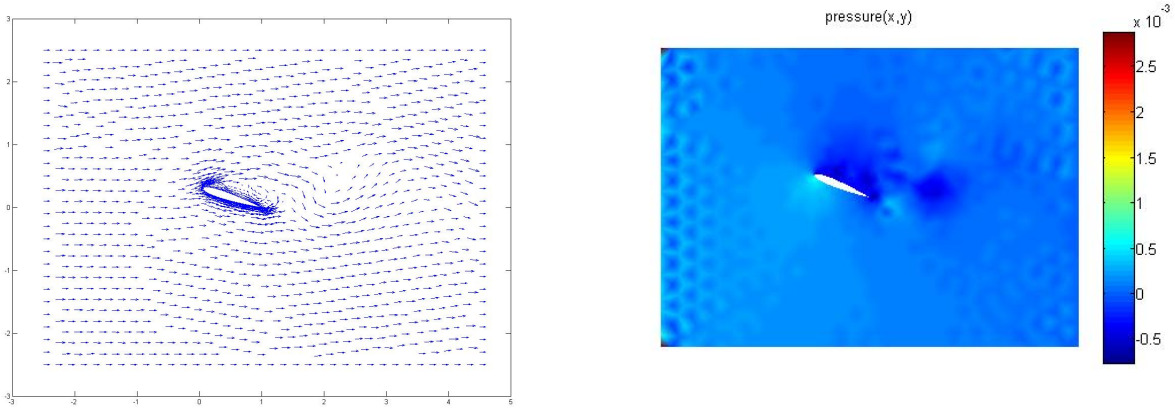

Figure 6. Velocity Vectors and Pressure Contours at 18 degrees pitching up

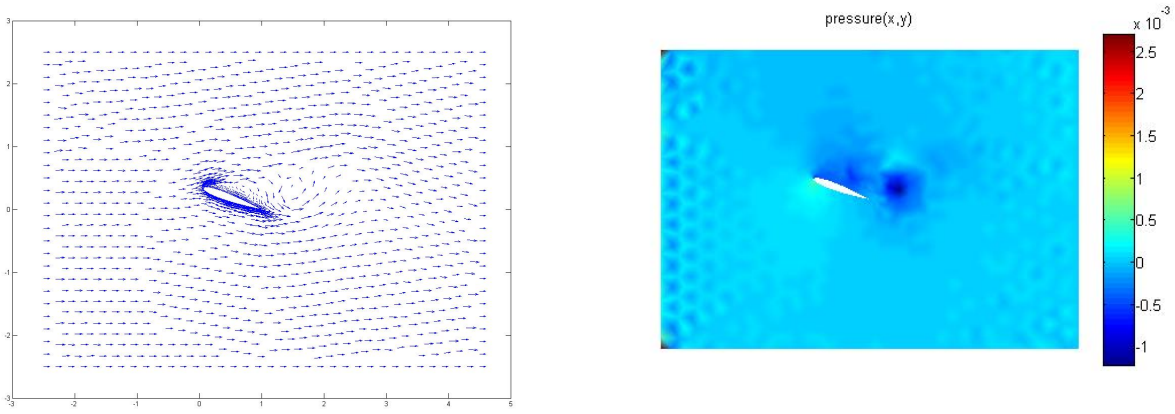

Figure 7. Velocity Vectors and Pressure Contours at 20 degrees pitching down

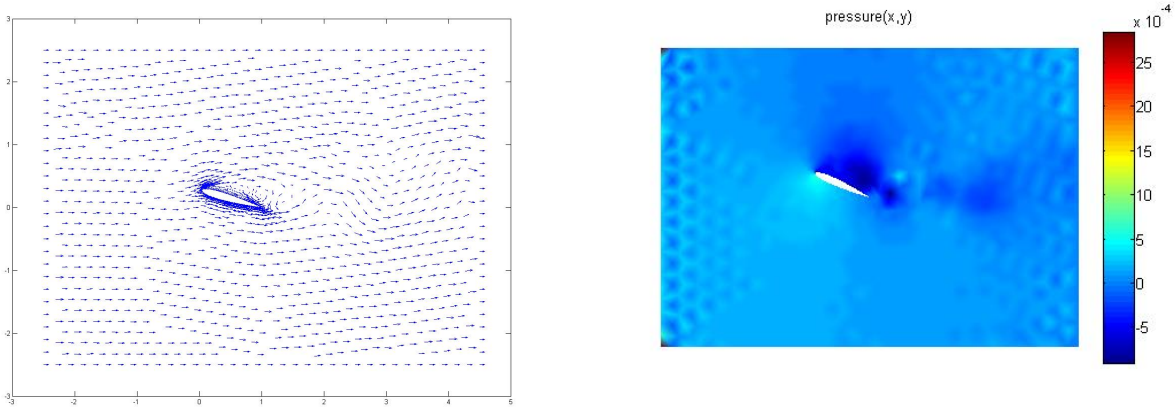

Figure 8. Velocity Vectors and Pressure Contours at 16 degrees pitching down

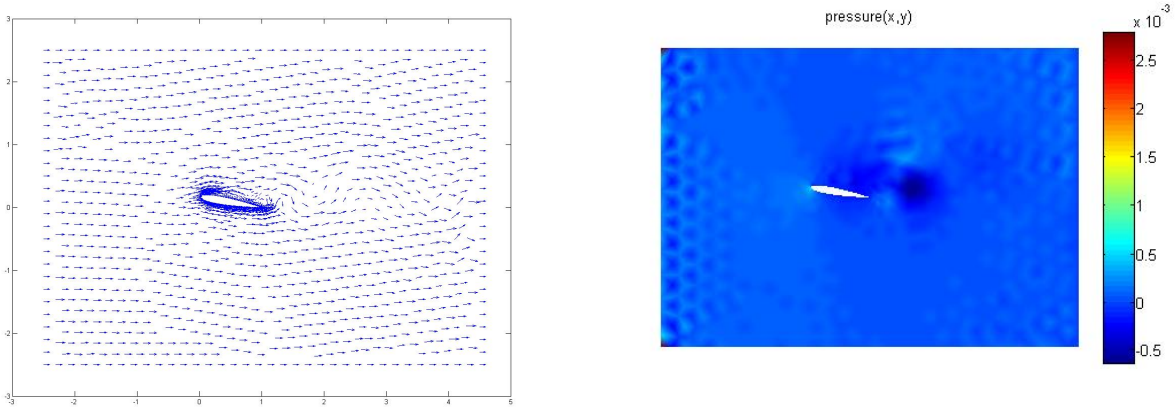

Figure 9. Velocity Vectors and Pressure Contours at 10 degrees pitching down

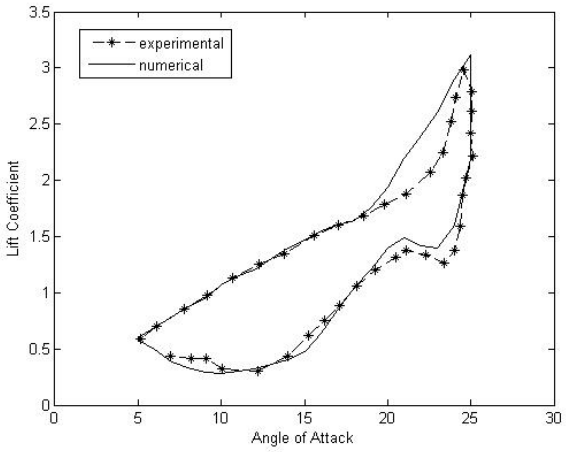

Figure 10. Dynamic Lift Coefficient Curve

5. CONCLUSIONS

Results of a finite numerical simulation of the laminar flow over an static and dynamic NACA 0012 airfoil were presented. Velocity vectors for observing flow topology and numerical-experimental comparing on the vertical force coefficient were performed.

The static case showed the typical airfoil flow pattern, where the vertical force coefficient was well predicted for angles below 8 degrees. For angles above that value, the numerical results are overestimated when compared with experimentation. The normal stall effects can explain that slight overestimation, since on that flow state, forces are influenced by the stall phenomena. The dynamic case had shown qualitative results of velocity vectors. Those results hold resemblance with experimental flow visualization available at the literature. Flow effects, such as vortex shedding, recirculation zones formation and shear layer shedding were observed.

The obtained results can be considered as good, but further analysis is needed for the characterization of the dynamic stall. In the future, moment coefficient values are intended to be calculated, and analysis of the damping effect of the flow on the airfoil will be analyzed.

6. REFERENCES

Zienkiewicz, O. C., Taylor, R. L., e Nithiarasu, P. The Finite Element Method for Fluid Dynamics. Elsevier, 6th edition, 2005b.

Zienkiewicz, O. C., Taylor, R. L., e Zhu, J. Z. The Finite Element Method: Its Basis and Fundamentals. Elsevier, 6th edition, 2005a.

W.Shyy,, Udaykumar, S., Rao, M. M., e Smith, R. W. Computational Fluid Dynamics with Moving Boundaries. McGraw-Hill, 6th edition, 2008.

Duan, Q. e Li, X. An ale based iterative cbs algorithm for non-isothermal non newtonian flow with adaptive coupled finite element and meshfree method. Computational Methods in Applied Mechanics and Engineering, 196:4911-4933, 2007.

Franca, L. P., Haukeb, G., e Masud, A. Revisiting stabilized finite element methods for the advective - diffusive equation. Computational Methods in Applied Mechanics and Engineering, 195:1560-1572, 2006.

Pereira, R. M. Simulação numérica de escoamentos laminares e turbulentos através do método dos elementos finitos com estabilização CBS. Dissertação de Mestrado, Universidade de Brasília, 2004.

Donea, J. e Huerta, A. Finite Element Method for Flow Problems. Wiley, 2003.

Svacek, P., Feistauer, M., e Horacek, J. Numerical simulation of flow induced airfoil vibrations with large amplitudes. Journal of Fluids and Structures, 23, 391-411, 2007.

Naudascher, E. and Rockwell, D. Flow Induced Vibrations: An Engineering Guide. Dover, 2005

Digavalli, S. Dynamic Stall of a NACA 0012 in Laminar Flow, PhD thesis, Massachussetts Institute of Technology 1993.

Fujisawa, N., Shibuya, S. Observations of dynamic stall on Darrieus wind turbine blades, Journal of Wind Engineering and Industrial Aerodynamics 89 201-214, 2001

Ekaterinaris, J. and Platzer, M. Computational Prediction of Airfoil Dynamic Stall, Progress on Aerospace Sciences, 33, 759-846, 1997.

J. T. Batina. Unsteady Euler algorithm with unstructured dynamic mesh for complex-aircraft aerodynamic analysis. AIAA Journal, 29(3):327-333, 1991.

B. Koobus C. Farhat, C. Degand and M. Lesoinne. An improved method of spring analogy for dynamic unstructured fluid meshes. In Proceedings of the 39th AIAA/ASME/ASCE/AHS/ASC structures, structural dynamics, and materials conference and exhibit, April 20-23, 1998, Long Beach, California.

C. Degand and C. Farhat. A three-dimensional torsional spring analogy method for unstructured dynamic meshes. Computers and Structures, 80:305-316, 2002.

C. Farhat, M. Lesoinne, and P. LeTallec. Load and motion transfer algorithms for fluid-structure interaction problems with non-matching discrete interfaces: Momentum and energy conservation, optimal discretization and application to aeroelasticity. Computer Methods in Applied Mechanics and Engineering, 157:95-114, 1998.

Chorin, A. J. (1968), "Numerical solution of the Navier-Stokes equations", Math. compt., 22: 745-762.

Codina, R., Blasco,J., "Stabilized finite element method for transient Navier-Stokes equations based on a pressure gradient projection" (2000), Comput. Methods Appl. Mech. Engrg., 182: 277-300.

Codina, R. (2000), "Pressure stability in fractional step finite element methods for incompressible flow", J. for Compt. Physics, 170: 112-140.

Codina, R. Houzeaux, G., Coppol-Owen, H., Baiges, J. (2009), The fixed-mesh ALE approach for the numerical approximation of flows in moving domains, J. of Compt. Physics, 228: 1591-1611.

Goldberg, D., Ruas, V. (1999), A numerical study of projection algorithms on finite element simulation of three-dimensional viscous incompressible flows, Int. J. Numer. Meth. Fluids, 30: 233-256.

Guermond, J.L., Minev, P., Shen, J. (2006), "An overview of projection methods for incompressible flows", Comput. Methods Appl. Mech. Engrg., 195: 6011-6045.

Lohner,R., Yang, C., Cebral, J., Camelli, F., Soto, O., Waltz, J. (2006), "Improving the speed and accurancy of projection-type incompressible flow solvers", Comput. Methods Appl. Mech. Engrg., 195: 3087-3109.

7. Responsibility notice

The author(s) is (are) the only responsible for the printed material included in this paper